Upper crustal structure of southwestern British Columbia from the 1998 Seismic Hazards Investigation in Puget Sound

K. Ramachandran,[1,2] S. E. Dosso,[1] C. A. Zelt,[3] G. D. Spence,[1] R. D. Hyndman,[1,4] and T. M. Brocher[5]

Received 5 October 2003; revised 20 March 2004; accepted 6 July 2004; published 9 September 2004.

[1] This paper applies nonlinear three-dimensional travel time tomography to refraction data recorded during the 1998 Seismic Hazards Investigation in Puget Sound (SHIPS) to derive the first large-scale, high-resolution upper crustal velocity model for southwestern British Columbia. A minimum structure *P* wave velocity model is constructed using 175,000 first arrival travel times picked from data recorded by 58 temporary onshore stations. The model details forearc crustal structures related to terrane accretion and subsequent basin formation to a depth of about 10 km. The Metchosin igneous complex (correlative with the Eocene Crescent-Siletz Terrane in Washington) is imaged as a laterally extensive WNW trending high-velocity anomaly underlying southernmost Vancouver Island and much of the Strait of Juan du Fuca. Northeast of the Strait of Georgia, the southwesterly dip of the contact between the Wrangellia terrane rocks of Vancouver Island and the Coast Plutonic Complex suggests Wrangellia rocks are down-faulted against the plutonic complex. At the southwestern end of the Strait of Juan de Fuca, the 50 km long WNW trending Clallam basin has a maximum thickness of 5–6 km. Near the eastern end of the Strait of Juan de Fuca, Port Townsend basin has an inferred thickness of approximately 4–5 km. The southern end of the 9 km thick Georgia basin is bounded by a high-velocity basement ridge. Beneath the Strait of Georgia, clusters of well-located earthquakes have a prominent NW trend and coincide spatially with rapid lateral velocity changes. Clusters of microearthquakes there are associated with the intersection of several east trending structural highs within this NW trend. *INDEX TERMS:* 7205 Seismology: Continental crust (1242); 7260 Seismology: Theory and modeling; 8180 Tectonophysics: Tomography; *KEYWORDS:* seismic tomography, wide-angle, Cascadia

Citation: Ramachandran, K., S. E. Dosso, C. A. Zelt, G. D. Spence, R. D. Hyndman, and T. M. Brocher (2004), Upper crustal structure of southwestern British Columbia from the 1998 Seismic Hazards Investigation in Puget Sound, *J. Geophys. Res.*, *109*, B09303, doi:10.1029/2003JB002826.

1. Introduction

[2] The potential occurrence of damaging earthquakes in southwest British Columbia and northwest Washington State led to the Seismic Hazards Investigation in Puget Sound (SHIPS) conducted in 1998 [*Fisher et al.*, 1999; *Brocher et al.*, 1999]. The main objectives of the experiment were (1) to map active fault zones in the subsurface, (2) to determine the thickness and properties of sedimentary rocks in Cenozoic basins that may affect strong ground shaking, and (3) to image subsurface geological structures that may control the distribution of earthquakes. The survey consisted of firing shots from a large marine air gun array in the Strait of Juan de Fuca, the Strait of Georgia, and Puget Sound, and recording the shots on temporary land stations in southwest British Columbia and northwest Washington (Figure 1). Wide-angle *P* wave arrivals recorded in southwest British Columbia and the northern Olympic Peninsula are used here for three-dimensional (3-D) tomographic velocity inversion.

[3] The present study area comprises southern Vancouver Island and the Straits of Georgia and Juan de Fuca and overlaps in part with several previous studies based on SHIPS data, as shown in Figure 1. *Zelt et al.* [2001] used first arrival travel times from 1998 SHIPS to construct a 3-D velocity model for the Georgia Strait. *Brocher et al.* [2001] constructed a detailed 3-D upper crustal velocity model for the Puget Sound region from SHIPS first arrival travel times. *Van Wagoner et al.* [2002] extended Brocher et al.'s work to 30 km depth using SHIPS first arrivals and earthquakes. The present study encompasses the margin region

[1]School of Earth and Ocean Sciences, University of Victoria, Victoria, British Columbia, Canada.
[2]Now at Pacific Geoscience Centre, Geological Survey of Canada, Sidney, British Columbia, Canada.
[3]Department of Earth Science, Rice University, Houston, Texas, USA.
[4]Pacific Geoscience Centre, Geological Survey of Canada, Sidney, British Columbia, Canada.
[5]U.S. Geological Survey, Menlo Park, California, USA.

0148-0227/04/2003JB002826$09.00

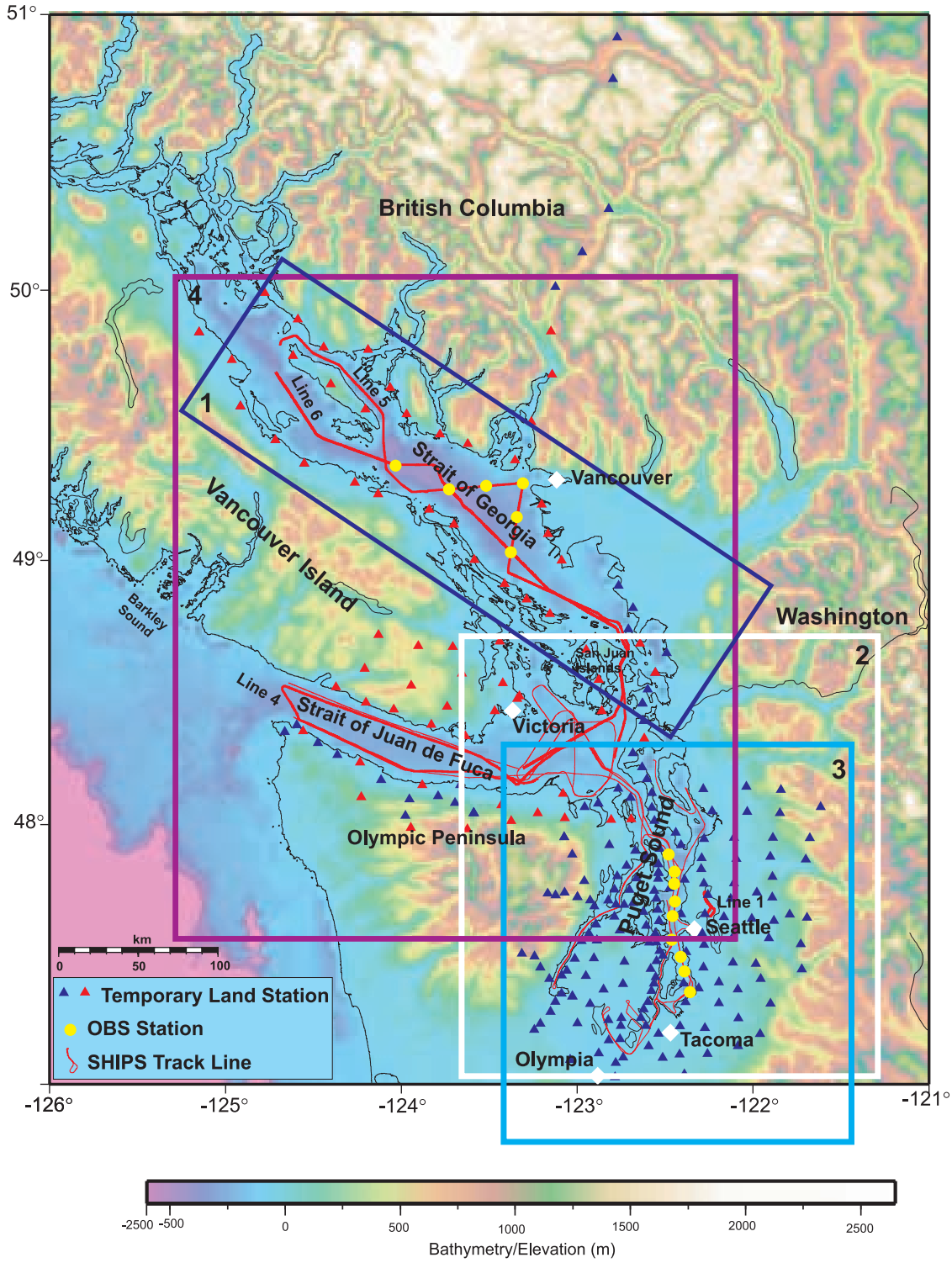

Figure 1. Location map showing the SHIPS shots (red lines) and receivers (blue and red triangles). The rectangular areas represent the tomographic study areas of (1) *Zelt et al.* [2001], (2) *Brocher et al.* [2001], and (3) *Van Wagoner et al.* [2002]. The study area of the work reported in this paper is represented by the rectangle (4). Red triangles show the receivers used in this study.

between 48°–50°N including most of the study area of *Zelt et al.* [2001] and overlapping the northern ends of the study areas of *Brocher et al.* [2001] and *Van Wagoner et al.* [2002]. The present study provides a high-resolution, 3-D velocity model of the forearc upper crust, composed of accreted terranes, beneath the Strait of Juan de Fuca, the Strait of Georgia, and southern Vancouver Island [*Ramachandran*, 2001].

[4] Small to moderate sized crustal earthquakes are concentrated in southwestern British Columbia and in the Puget

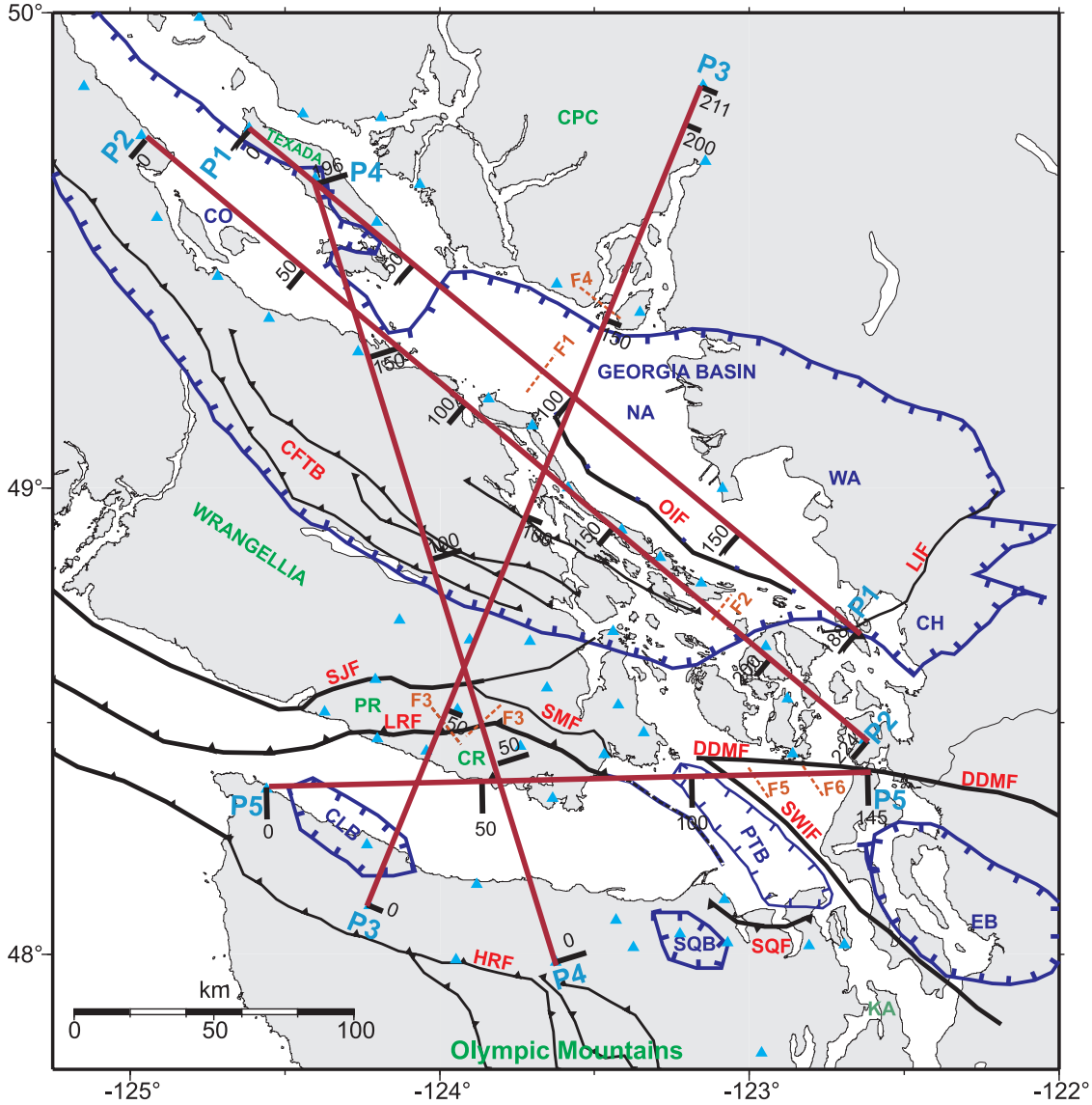

Figure 2. Sedimentary basin and fault map. Major geologic features taken from *Muller* [1977], *England and Bustin* [1998], *Brocher et al.* [2001], and *Van Wagoner et al.* [2002]. CFTB, Cowichan Fold and Thrust Belt; CH, Chuckanut subbasin; CLB, Clallam basin; CO, Comox subbasin; CPC, Coast Plutonic Complex; CRBF, Coast Range boundary fault; CR, Crescent terrane; DDMF, Darrington-Devils Mountain fault; EB, Everett basin; HCF, Hood Canal fault; HRF, Hurricane Ridge fault; LIF, Lummi Island fault; LRF, Leech River fault; NA, Nanaimo subbasin; OF, Olympia fault; OIF, Outer Islands fault; PR, Pacific Rim terrane; PTB, Port Townsend basin; SB, Seattle basin; SF, Seattle fault; SJF, San Juan fault; SMF, Survey Mountain fault; SQB, Sequim basin; SQF, Sequim fault; SU, Seattle uplift; SWIF, Southern Whidbey Island fault; TB, Tacoma basin; TF, Tacoma fault; WA, Whatcom subbasin. P1, P2, P3, P4, and P5 show the location of the vertical cross sections shown in Figure 7. F1 to F6 are probable fault locations identified on the vertical cross sections.

Lowland. These are limited to the upper 30 km of the continental crust, constrained by the maximum temperature for brittle failure of about 350°C [*Hyndman and Wang*, 1993]. These earthquakes are driven, in part, by a margin-parallel compressive stress [e.g., *Wang et al.*, 1995]. Few correlations of surface faulting with seismicity have been reported in the study region, except for the probable association of the 1946, M = 7.3 event with the Beaufort Range fault or subsidiary faults in central Vancouver Island [*Rogers and Hasegawa*, 1978] and an active fault in the northern Georgia Strait [*Cassidy et al.*, 2000; *Mosher et al.*, 2000].

2. Geology and Tectonics

[5] Most of southwestern British Columbia is made up of the Insular belt comprising Wrangellia rocks [*Muller*, 1977]. Around mid-Cretaceous time, the Insular Superterrane was emplaced against the existing continental margin

represented by the Intermontane superterrane, and generated the mid-Cretaceous to early Tertiary intrusive rocks of the Coast Belt over the region of the suture [*Monger et al.*, 1982]. Georgia Basin overlaps the Coast and Insular belts (Figure 2) and the structure of these belts is considered to be a stack of northeast dipping underthrust sheets of late Jurassic to Holocene crust [*Engebretson et al.*, 1985; *Monger*, 1990]. The eastern extent of Wrangellia rocks and the nature of the contact with the rocks of the Coast Belt may vary along the boundary between the Insular and Coast belts [*Clowes et al.*, 1997]. The basement rocks and their sedimentary cover are involved in the deformation, and the majority of the structures are Eocene, coincident with the accretion of Pacific Rim and Crescent terranes to Wrangellia [*Engebretson et al.*, 1985; *Clowes et al.*, 1987; *England and Calon*, 1991]. On southern Vancouver Island, the Pacific Rim terrane is separated from Wrangellia by the San Juan and Survey Mountain faults (Figure 2). The Pacific Rim terrane is also exposed in a narrow strip along the central west coast of the Island, bounded on the east by the West Coast fault. Metchosin volcanics of southern Vancouver Island are considered to be correlative with mafic volcanic rocks of the Eocene Crescent Formation of the Olympic peninsula, composed of basalt, diabase, and gabbro [*Muller*, 1980] and the Siletz terrane of Coastal Oregon. On southern Vancouver Island the Leech River fault bounds the Pacific Rim and Crescent terranes. To the south of Vancouver Island, the Strait of Juan de Fuca is underlain in part by a thick section of sedimentary rocks that lie in a synclinal depression formed in the Crescent terrane. To the east of Vancouver Island, the Strait of Georgia, a large forearc basin, straddles the boundary between the Insular and Coast belts.

3. Seismic Hazards Investigation in Puget Sound

[6] The SHIPS experiment recorded arrivals from a total of 33,000 air gun shots fired on 11 shot lines in the waterways of the Strait of Georgia, the Strait of Juan de Fuca, and Puget Sound (Figure 1). The shots were recorded at 257 temporary land-based Reftek stations [*PASSCAL*, 1991] and 15 ocean bottom seismometers at offsets from 1 to 370 km [*Brocher et al.*, 1999]. The receiver locations were distributed widely over southwestern British Columbia and northwestern Washington, as shown in Figure 1. For this work, first arrival travel times were picked from four shot lines (lines 1, 4–6 on Figure 1) providing a total of 12,457 shots. Data processing included applying a 4–15 Hz band-pass filter to remove high-frequency noise and enhance the time sections for first break identification and picking. Processed record sections for station CA04, for an east trending line in the Strait of Juan de Fuca (Figures 3a and 3b) and a north trending line in the Strait of Georgia (Figures 3c and 3d), provide examples of high and average quality data. First arrivals were picked manually. Approximately 175,000 first arrival times were made from 58 receivers amounting to 24% of the available shots.

[7] Line 1, located in Lake Washington in Seattle, was usefully recorded by receivers on the Olympic Peninsula and southern Vancouver Island. Line 4, recorded by receivers in southern Vancouver Island, Olympic Peninsula, and portions of mainland British Columbia, provided high-quality travel time picks. Lines 5 and 6 produced intermediate quality picks, mostly from receivers on southern Vancouver Island. Pick uncertainties of 50, 70, and 90 ms were assigned to picks having first arrival travel times less than 10 s, 10–15 s, and greater than 15 s, respectively. These unreduced travel times correspond to source receiver offsets less than 65 km, 65–100 km, and greater than 100 km, respectively.

4. Modeling Procedure

[8] We apply the regularized inversion described by *Zelt and Barton* [1998] and briefly summarize the methodology here. Computation of travel times in a velocity model is the forward step of the inverse problem. *Vidale*'s [1990] method calculates first-arrival travel times on a uniform grid by solving the Eikonal equation using the finite difference method. The velocity model is defined at the nodes of a uniformly spaced grid and the finite difference method is used to compute travel times at the nodes. The travel time at a particular receiver location is then obtained by linear interpolation of the travel times at the eight surrounding grid nodes. To compute the ray path length, the gradient direction from the receiver to the source is traced in the travel time grid. This tomographic inversion method is based on iterative linearized inversion of the travel time equations, regularized by minimizing the vertical and horizontal roughness subject to fitting the data to within estimated uncertainties using the χ^2 criterion. For data with independent Gaussian errors, the acceptable data misfit is set to the expected value for the χ^2 misfit statistic, i.e., $\Delta\mathbf{t}^T\mathbf{C}_d^{-1}\Delta\mathbf{t} = N$, where N is the number of data and $\mathbf{C}_d$ is a diagonal matrix with elements σ_i^2 representing the variance of the ith travel time measurement. The normalized χ^2 is defined as $\Delta\mathbf{t}^T\mathbf{C}_d^{-1}\Delta\mathbf{t}/(N-1)$. From *Zelt and Barton* [1998], the solution at each iteration was obtained by solving the system of equations

$$\begin{bmatrix} \mathbf{C}_d^{-1/2}\mathbf{L} \\ \lambda\mathbf{C}_h \\ s_z\lambda\mathbf{C}_v \end{bmatrix} \Delta\mathbf{m} = \begin{bmatrix} \mathbf{C}_d^{-1/2}\Delta\mathbf{t} \\ -\lambda\mathbf{C}_h\mathbf{m}_\circ \\ -s_z\lambda\mathbf{C}_v\mathbf{m}_\circ \end{bmatrix}, \quad (1)$$

where $\Delta\mathbf{m}$ is the perturbation to the current slowness vector model $\mathbf{m}_\circ$; $\Delta\mathbf{t}$ is the travel time residual vector; $\mathbf{C}_h$ and $\mathbf{C}_v$ are the horizontal and vertical roughening matrices, respectively; λ is the trade-off parameter; s_z controls the relative importance of vertical to horizontal model smoothness; $\mathbf{L}$ is the partial derivative matrix with elements $L_{ij} = \partial t_i/\partial m_j$ equal to the length of the ith ray in the jth cell of the slowness model; and $\mathbf{m} = \mathbf{m}_\circ + \Delta\mathbf{m}$ is the updated slowness model.

[9] The velocity model, for both forward and inverse steps, was parameterized by a node/cell spacing of (1 × 1 × 1) km in the (x, y, z) directions. The velocity model dimensions were (220 × 220 × 22) km. The top of the model was set to 1 km above sea level to allow the positioning of receivers at their actual elevations. An initial velocity model in one-dimension (Figure 4a) was constructed that best fit the time-distance plot and that was consistent with the regional geology. The travel time misfit for the picks in

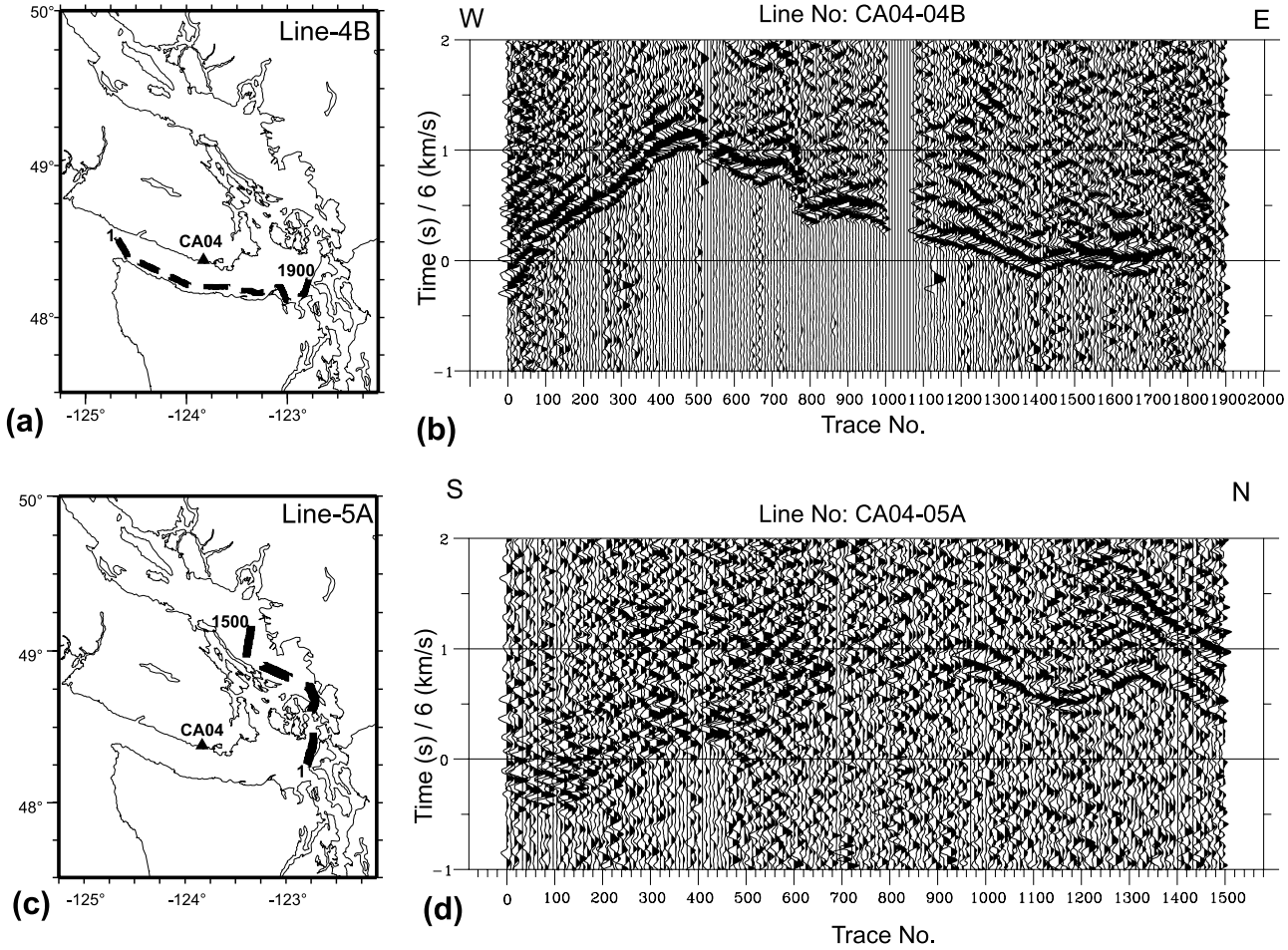

Figure 3. Location map of the shot line segments 4B and 5A (a and c) and the corresponding time sections recorded by the receiver CA04 (b and d). Location of the receiver CA04 is shown by the black triangle. Data are plotted with a reducing velocity of 6 km/s.

the initial model are shown in Figure 4b. Large travel time misfits (±1.5 s) at some offsets are explained by strong lateral variations in subsurface geology.

[10] The horizontal and vertical smoothing applied here is described by *Zelt and Barton* [1998]. The inversion procedure was initially run in test mode to determine an appropriate value for the ratio of vertical to horizontal smoothing parameter s_z. During this testing outliers in the travel time picks were identified and removed. These outliers, caused by errors in manual picking, amounted to <1% of the data used in the inversion. Several values of s_z were tested and the resulting velocity models were analyzed for smoothness, continuity, and correlation with known geological features. The final model obtained from the inversion with a value of 0.25 for s_z was consistent with the present knowledge of the regional geology and comparable to velocity data obtained from previous studies in the region by *Zelt et al.* [2001]. The value of s_z was held fixed throughout the inversion.

[11] The parameter λ acts as a trade-off between data misfit and model smoothness. For large λ, model smoothness is emphasized over fitting the data; as λ decreases, the relative importance of fitting the data increases. During the inversion procedure, λ is tested over a range of values by slowly decreasing it from a starting value, and the value that achieves the smallest data misfit $\Delta\mathbf{t}^T\mathbf{C}_d^{-1}\Delta\mathbf{t}$ is selected for that iteration. The starting value of λ and the reduction factor were chosen such that small steps were taken in the model space to honor linearization. The RMS travel time residual for the starting model for 1.7×10^5 picks was 549 ms for a normalized χ^2 of 73. After six iterations of the linearized inversion the RMS travel time misfit reached a stable minimum of 76 ms for a normalized χ^2 of 1.04. The travel time misfit for the final model is uniform over the entire range of offsets as shown in Figure 4c.

5. Ray Coverage and Checkerboard Tests

[12] In evaluating constructed velocity models, it is important to consider model resolution, that is, how well individual model parameters are determined. In the case of perfect model resolution, each model parameter is determined independently from all other model parameters. As resolution decreases, averages of neighboring parameters can be estimated but not the individual parameters themselves. The simplest method to evaluate resolution is ray hit count analysis in which the number of rays passing through a given cell are examined, and reasonable resolution is inferred for regions with sufficient ray coverage [*Toomey et al.*, 1994; *Parsons et al.*, 1996].

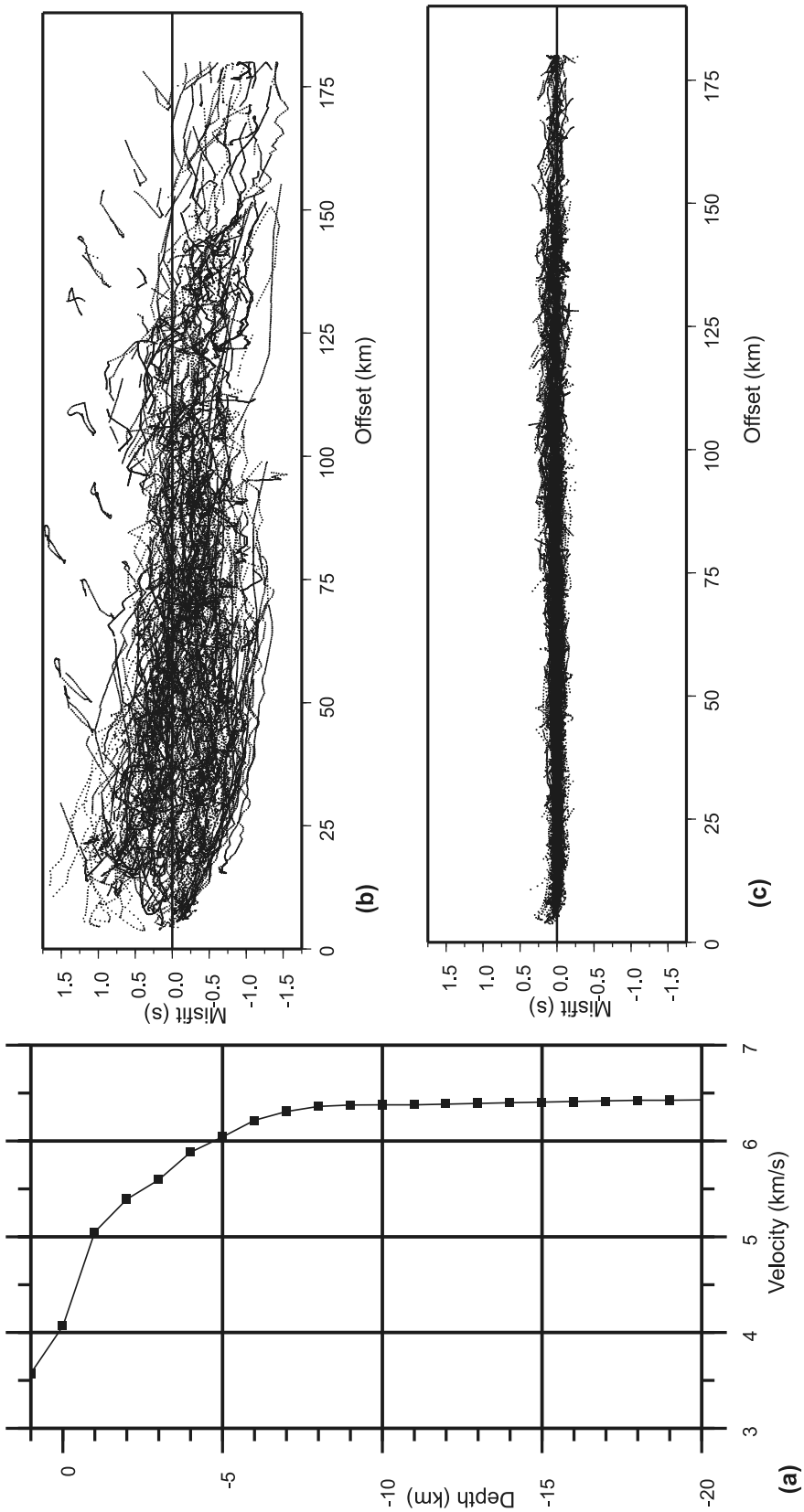

Figure 4. (a) Starting 1-D velocity model. (b) Travel time misfit for initial 1-D velocity model. (c) Travel time misfit for final 3-D velocity model.

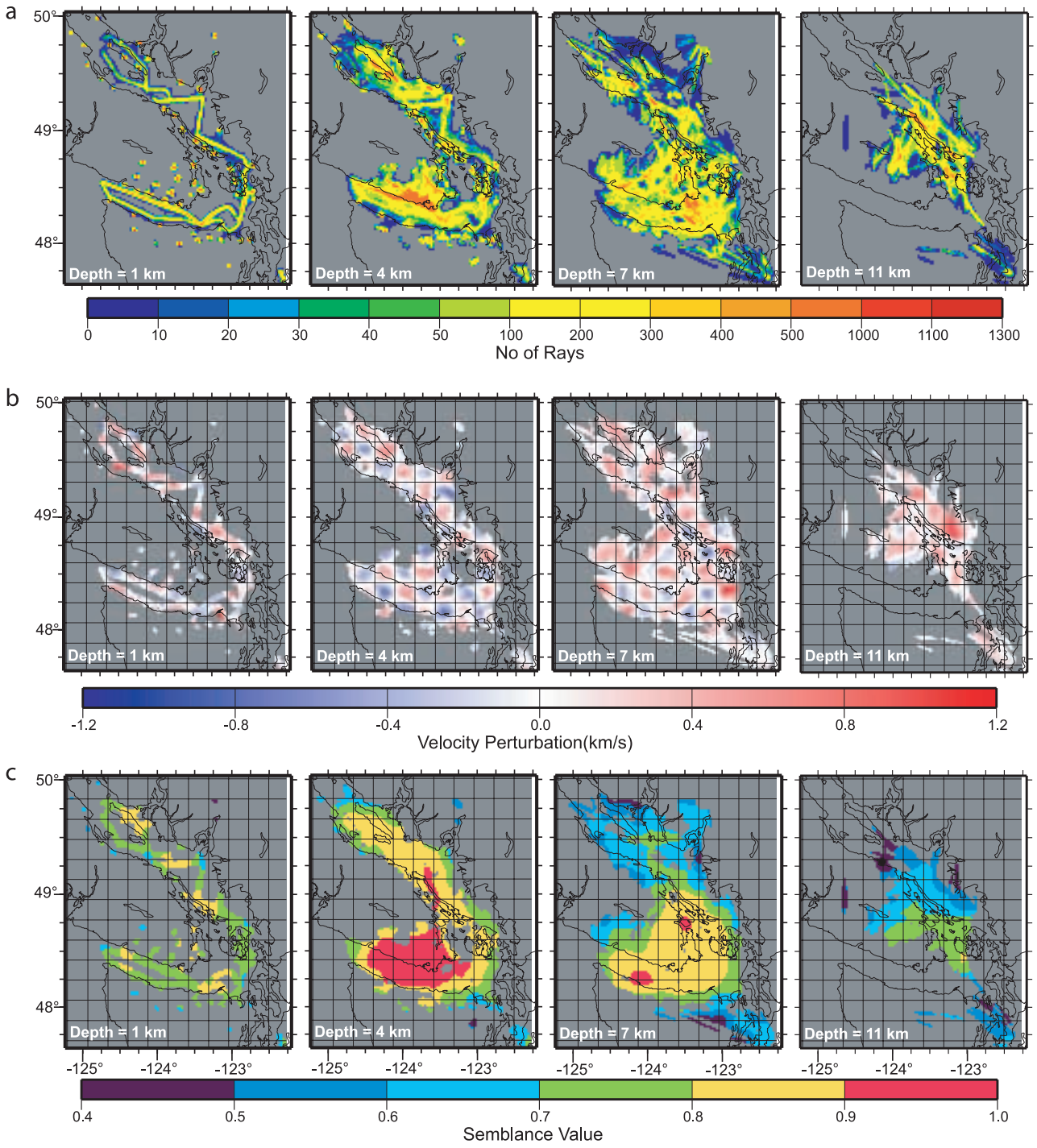

Figure 5. (a) Depth slices of ray density in the final velocity model at 1, 4, 7 and 11 km depth. (b) Depth slices of checkerboard test recovered anomaly pattern for 20 km grid size at 1, 4, 7, and 11 km depth. (c) Depth slices of semblance values for 20 km checkerboard grid size at 1, 4, 7, and 11 km depth.

[13] To apply this method, rays were traced though the final velocity model to determine the number of rays/cell, and are shown in Figure 5. Model parameters are plotted only for cells having ray coverage, amounting to about 14% of the model volume. Ray coverage varies with depth and generally is a maximum at approximately 7 km depth (Figure 5a). In the Straits of Georgia and Juan de Fuca, the ray coverage is sufficient to clearly map the thickness of lower-velocity sediments and associated structural features. Because of the geometry of the SHIPS experiment, the ray coverage at depths shallower than 4 km is confined mostly to these Straits. Ray coverage in southern Vancouver Island extends downward to a maximum depth of 11 km. Strong ray focussing occurs in the Crescent terrane beneath south-

ern Vancouver Island (Figure 5a). In the Strait of Georgia, reasonable ray coverage is observed at all levels to 11 km depth.

[14] Another method to assess model resolution is the checker board test [e.g., *Humphreys and Clayton*, 1990; *Hearn and Ni*, 1994; *Zelt and Barton*, 1998]. Using the approach of *Zelt and Barton* [1998], a synthetic velocity model is generated by the addition of a laterally alternating anomaly pattern of positive and negative squares to the final model obtained by inversion. The anomaly pattern varies in the horizontal but not in the vertical direction. The source-receiver geometry of the experiment is then used to compute synthetic travel times. Gaussian noise with a standard deviation equal to the estimated uncertainties in the travel time picks is added to the computed travel times. The synthetic travel time data are then inverted using the final inversion model as the starting model. By assessing the recovered anomaly pattern, an estimate of the ability of the data to resolve anomalies with a lateral dimension equal to the size of the anomaly pattern can be obtained throughout the model. Reasonable ray coverage will generally enable the recovery of the alternating anomaly pattern. Regions of poor ray coverage typically result in a smooth nonalternating recovered pattern due to the horizontal smoothing included in the inversion.

[15] Semblance values measuring the correlation between the input and recovered patterns are used to classify model volumes having reasonable lateral resolution. As described by *Zelt and Barton* [1998], semblance is given by

$$S = \frac{1}{2}\frac{\sum_{i=1}^{I}\sum_{j=1}^{J}\sum_{k=1}^{K}\left[vt_{i,j,k} + vr_{i,j,k}\right]^2}{\sum_{i=1}^{I}\sum_{j=1}^{J}\sum_{k=1}^{K}\left[vt_{i,j,k}^2 + vr_{i,j,k}^2\right]}, \qquad (2)$$

where $vt_{i,j,k}$ and $vr_{i,j,k}$ represent the velocity of the node in the input checkerboard model and the recovered checkerboard model, respectively, and (I, J, K) represent the number of cells in the semblance window in (x, y, z). Semblance values of 1 and 0.5 indicate total recovery of the perturbation and no recovery of the perturbation, respectively.

[16] The lateral resolution of the constructed velocity model was tested using checkerboard grid sizes of 20 km and 30 km. The smallest lateral resolution is expected to lie within this range, considering that the SHIPS receivers were separated by about 15 km on average. The recovered anomaly pattern for the 20 km cell size and the semblance values computed for a window size of (20 × 20 × 2) km are shown in Figures 5b and 5c, respectively. *Zelt and Barton* [1998] characterize semblance values of 0.7 and above as well resolved. Using this measure, the recovery of the alternating anomaly pattern for the 20 km grid pattern is reasonable to 9 km depth in most parts of the study area, as indicated by semblance values of 0.7 and above (Figure 5c). These results imply lateral resolution of 20 km scale features down to 9 km depth.

6. Interpretation

[17] The 3-D tomographic velocity model is interpreted here using horizontal velocity slices at 2 km intervals (Figures 6a–6f), vertical velocity slices (Figures 7a–7e), and isovelocity surfaces (Figures 8a and 8b). Horizontal and vertical velocity slices identify major structural trends and subsurface geometries within the upper crust. Isovelocity surfaces map structural boundaries, primarily the base of sedimentary basins. Hypocentral positions of earthquakes recorded between 1997 and 2001 are potted on each section (source is the Earthquake Catalogue 2001, Pacific Geoscience Centre, Geological Survey of Canada).

6.1. Seismic Velocities

[18] Previous studies guide our lithologic interpretation of the P wave velocity model. *Zelt et al.* [2001] proposed that beneath the Strait of Georgia velocities of 4.5–6.0 km/s represent deformed but little metamorphosed Upper Cretaceous Nanaimo Group sedimentary rocks. Beneath the southern Strait of Georgia, lower velocities in the shallower basin are associated with thicker horizons of Tertiary and younger overlying sedimentary rocks and deposits, including glacial and Holocene Fraser River deposits. In general, we consider velocities up to 5.5 km/s to represent sedimentary rocks. Deeper Cretaceous sedimentary rocks in the Nanaimo basin may have velocities up to 6.0 km/s due to compaction and lithification.

[19] Reported seismic velocities in deeper Wrangellia rocks vary from 6.4 to 6.75 km/s [*McMechan and Spence*, 1983; *Spence et al.*, 1985; *Zelt et al.*, 2001]. However, shallower Wrangellia rocks, down to about 2 km depth, have lower velocities (5.5 to 6.0 km/s) resulting from weathering and fracturing [*Zelt et al.*, 2001]. The Pacific Rim terrane along the west and southern parts of Vancouver Island is composed of sedimentary, metamorphic, and volcanic rocks having a velocity range from 6.0 to 6.2 km/s [e.g., *Clowes et al.*, 1987].

[20] *Van Wagoner et al.* [2002], examined borehole and laboratory measurements of P wave velocities, and concluded that the expected range of velocity in the Crescent Formation was 4.5–5.5 km/s for depths less than 5 km and 5.5–6.5 km/s at greater depth. Laboratory P wave velocities for Crescent Formation basalts from western Washington vary from 5.8 to 6.2 km/s over confining pressures corresponding to depths up to 7 km [*Brocher and Christensen*, 2001]. Gabbro members of the Crescent Formation have P wave velocities ranging up to 6.9 km/s [*Brocher and Christensen*, 2001]. The uncertainty in the velocities of the various rock types reported above, to a depth of 10 km, is expected to be ±0.2 km/s.

6.2. Sedimentary Basins

[21] Four large sedimentary basins are mapped here on the basis of their low seismic velocities and closed velocity contours. These include the Clallam, Port Townsend, and Sequim Basins along the Strait of Juan de Fuca, and the Georgia Basin in the Strait of Georgia.

6.2.1. Clallam Basin

[22] Located near the western end of the Strait of Juan de Fuca, the Clallam basin, approximately 50 km long, trends in a WNW direction (Figures 6a, 6b, and 6c). The basin extends to a maximum depth of 5–6 km (Figures 6c, 7d, and 8a), and is underlain by Crescent Formation rocks having velocities greater than 6.0 km/s (Figure 7d). The low velocities defining the basin coincide with a gravity anomaly low (Figure 8c).

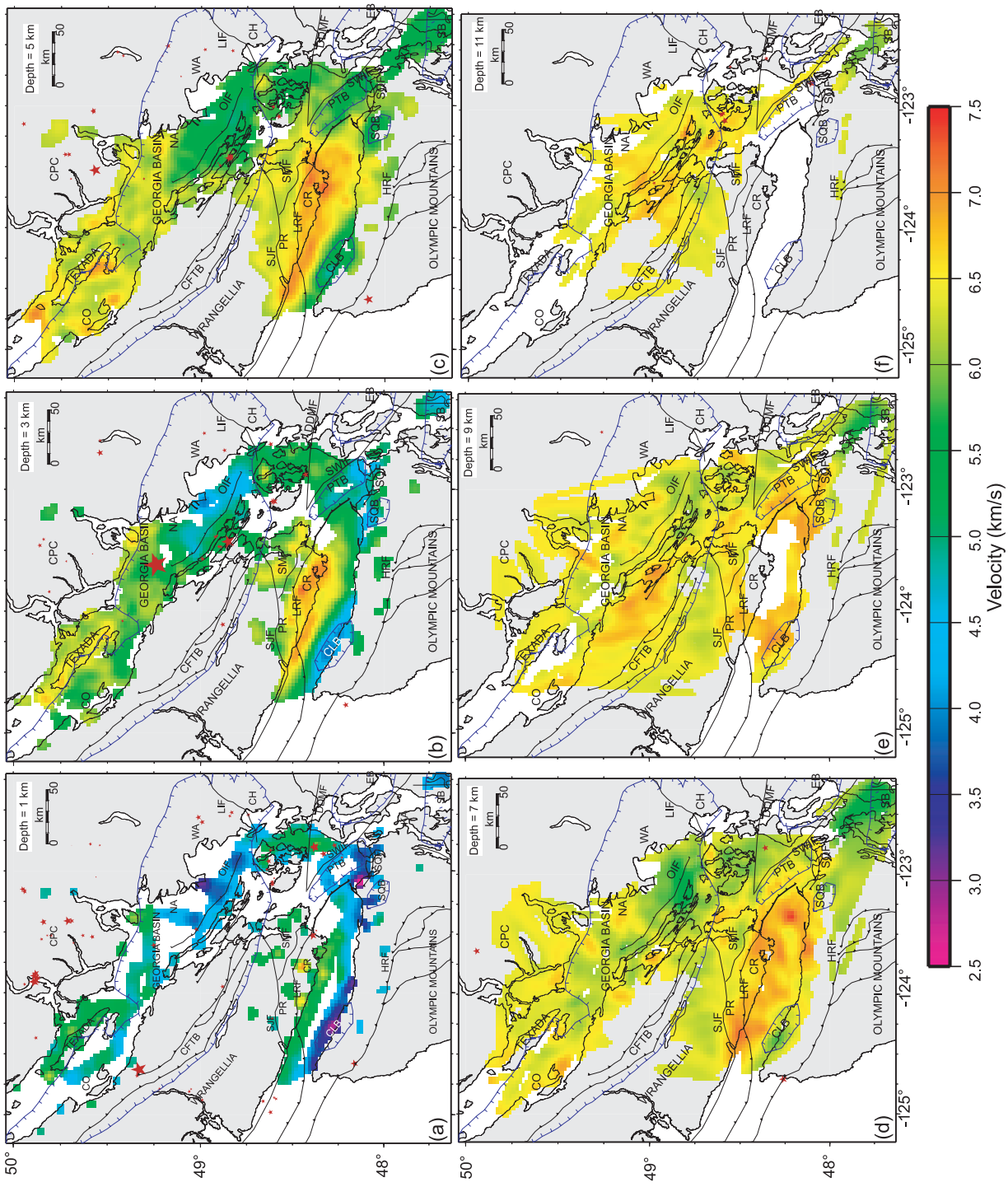

Figure 6. Depth slices of final velocity model at (a) 1, (b) 3, (c) 5, (d) 7, (e) 9, and (f) 11 km depth. Abbreviations are as in Figure 2.

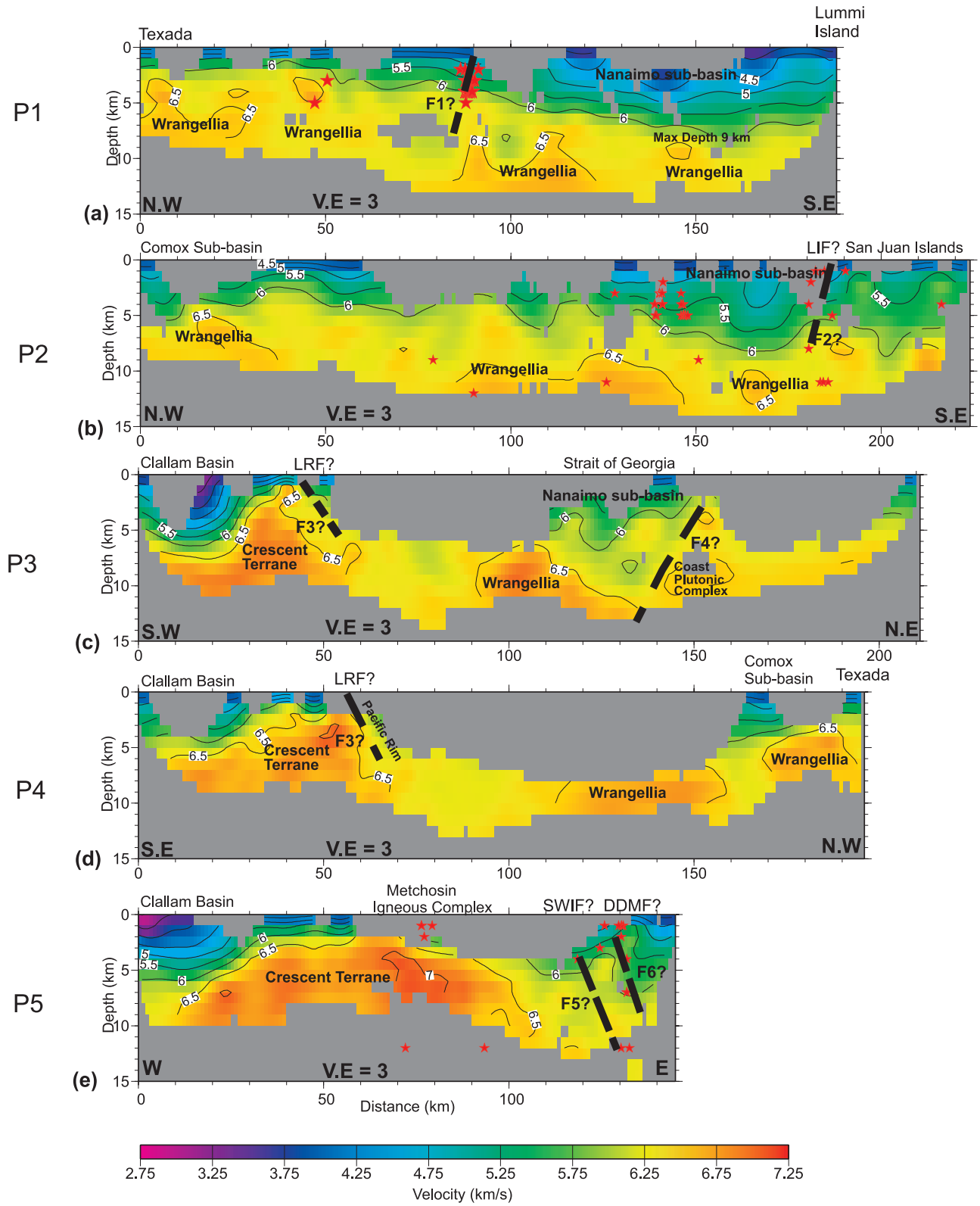

Figure 7. (a) Vertical velocity section P1. (b) Vertical velocity section P2. (c) Vertical velocity section P3. (d) Vertical velocity section P4. (e) Vertical velocity section P5. Earthquakes in the study region between 1997 and 2001 are shown as red stars. Abbreviations are as in Figure 2.

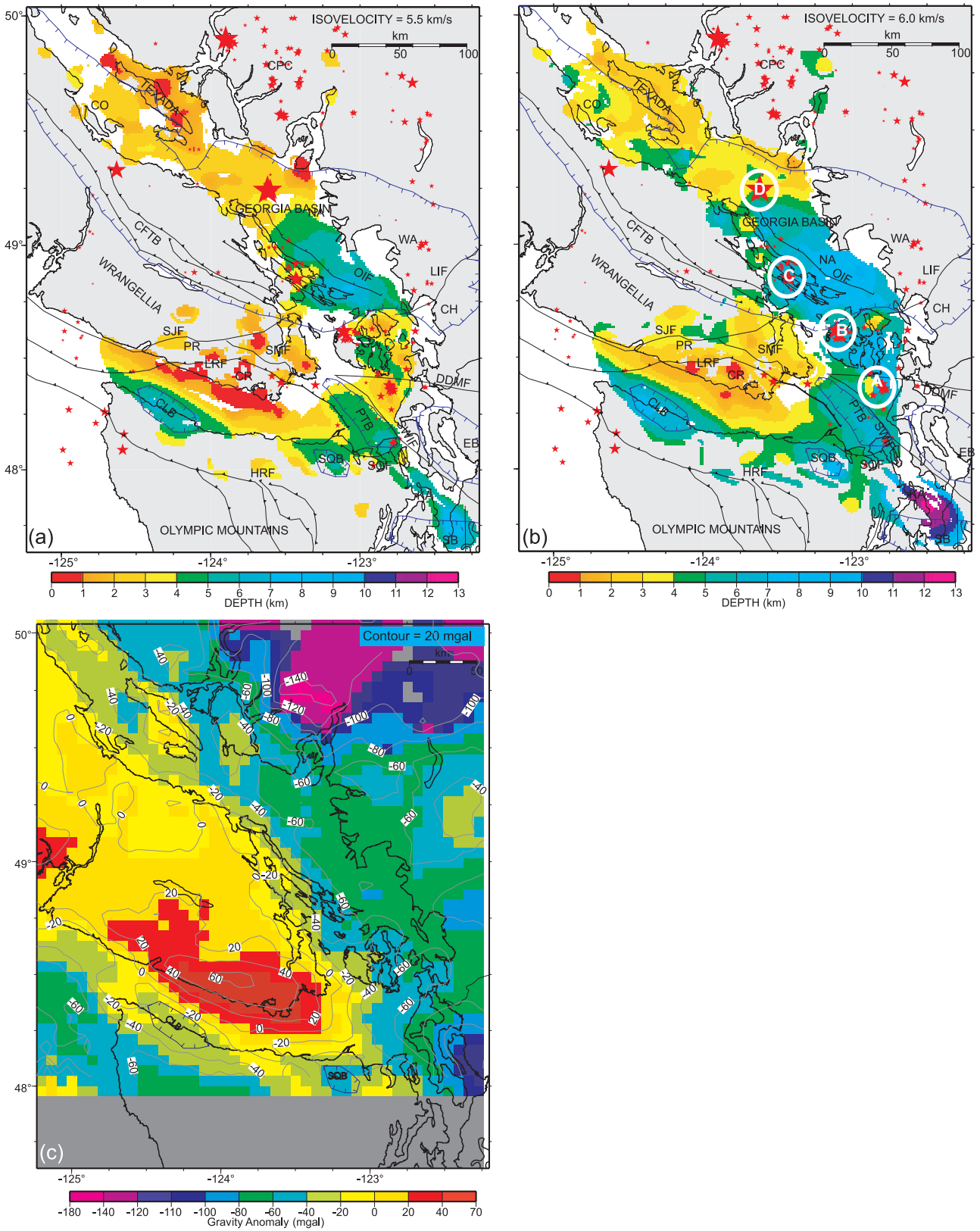

Figure 8. (a) Isovelocity surface map at 5.5 km/s. (b) Isovelocity surface map at 6.0 km/s. (c) Gravity anomaly map (Bouguer anomaly on land and free-air anomaly over ocean). Earthquakes between 0 and 12 km depth are shown as red stars. Abbreviations are as in Figure 2.

[23] This basin was first studied using 1998 SHIPS data by *Tréhu et al.* [2002]. Two industry test wells, located in the southeastern end of the basin, penetrated 1.8 and 2.2 km of sedimentary basin fill having sonic velocities less than 3.5 km/s without reaching Crescent Formation basement [*Brocher and Ruebel*, 1998]. The basin is bounded to the south by exposures of the Crescent Formation; its late Eocene and younger subsidence may reflect contractural deformation of the coast ranges associated with N–S compression [*Johnson et al.*, 1996; *Khazaradze et al.*, 1999].

6.2.2. Port Townsend Basin

[24] Low-velocity anomalies identify a basin at the eastern end of the Strait of Juan de Fuca in horizontal slices and isovelocity surfaces (Figures 6a, 6b, and 8a). *Brocher et al.* [2001] informally referred to this velocity low as Port Townsend Basin. The basin is less extensive laterally than the Clallam basin and has a maximum thickness of approximately 4–5 km (Figure 8a). Its chief importance is that, as a fault bounded basin, it locally defines the location of the Leech River fault to the southwest and the Southern Whidbey Island fault to the northeast (Figure 8a).

6.2.3. Sequim Basin

[25] Southwest of Port Townsend basin and the Sequim fault, a velocity low defines the Sequim basin (Figures 6a, 6b, and 8a). This small basin, informally named by *Van Wagoner et al.* [2002], has a maximum thickness of about 4 km and coincides with a small gravity low (Figure 8c).

6.2.4. Georgia Basin

[26] The Strait of Georgia is a topographic low in the forearc occupied by the Georgia basin, filled by Cretaceous to Holocene sedimentary rocks. Down to 3 km depth (Figures 6a and 6b) velocities in the northwestern end of the basin are generally higher than those to the southeast. At 5 km depth (Figure 6c) an east trending velocity high divides the northwestern and southeastern ends of the basin. In the southeastern end of the basin, vertical sections and isovelocity maps (Figures 7a, 7b, and 8a) image a 9 km thick sedimentary section filling the Nanaimo subbasin between 48.7°N and 49.25°N, assuming that the top of basement is represented by the 6.0 km/s contour. On an isovelocity map (Figure 8a), an east trending high at the northern edge of the Nanaimo subbasin coincides with the location of earthquake activity. The basement structure beneath the Nanaimo subbasin differs beneath sections P1 and P2.

[27] The Comox subbasin, located at the northwestern end of the Georgia strait, is considerably thinner than the Nanaimo subbasin. Its maximum thickness is about 3–4 km (Figure 7a), consistent with results reported by *Zelt et al.* [2001].

[28] Although the Georgia Basin is considerably larger and older than the Seattle basin [*Brocher et al.*, 2001], the Georgia and Clallam basins suggest that the series of east trending basins and basement highs observed in Puget Sound extends to the north and west. *Brocher et al.* [2001] identified the east trending Tacoma basin, Seattle uplift, Seattle basin, Kingston Arch, and Everett basin from their tomographic inversion of the 1998 SHIPS data. The east trending Clallam and Georgia basins, and the east trending high-velocity basement ridge in the San Juan Islands, indicate that this structural style may extend to the north of the Everett basin.

6.3. Upper Crust

6.3.1. Crescent Terrane

[29] On the basis of our velocity model, the Crescent terrane underlies an extensive area of southern Vancouver Island and adjoining areas in the Strait of Juan de Fuca and is much more laterally extensive in the subsurface than suggested by its limited area of outcrop (Figures 6a–6e). At 5 km depth the Crescent terrane, mapped beneath southern Vancouver Island from its high velocities of 6.5–7.0 km/s (Figure 6c), extends to the southeast and northwest from its exposure, as was also inferred from LITHOPROBE Vibroseis data [*Clowes et al.*, 1987]. At depth this terrane underlies the eastern end of the Strait of Juan de Fuca. In isovelocity maps (e.g., Figure 8b), the shallow depth to the top of the Crescent terrane correlates with exposures of basalts and gabbros of the Metchosin Igneous Complex on southern Vancouver Island [*Massey*, 1986]. Cross sections (Figure 7e) image the Crescent terrane down to 10 km depth and suggest that the Crescent terrane extends below this depth. The widespread occurrence of the Crescent terrane in our study area complements its prevalence in the Puget Lowland [*Brocher et al.*, 2001].

[30] Lateral velocity contrasts within the Crescent terrane indicate compositional/structural variation (e.g., Figure 6d). Higher velocity rocks of approximately 7 km/s occurring at depths as shallow as 3 km (Figure 8b) spatially correlate with exposures of gabbroic rocks and a gravity high (Figure 8c). Laboratory *P* wave velocities for gabbro from Crescent Formation rocks of western Washington vary from 6.6 to 6.8 km/s over confining pressures corresponding to depths extending from the surface to 7 km [*Brocher and Christensen*, 2001]. Measured *P* velocities in samples from the Crescent Formation near Olympia, Washington, ranged from 5.88 to 6.94 km/s [*Williams et al.*, 2001]. *Christensen and Mooney* [1995] observed gabbro *P* wave velocities to vary from 7.0 to 7.2 km/s over depths ranging from the surface to 10 km.

6.3.2. Pacific Rim Terrane

[31] In southern Vancouver Island, the contact between higher-velocity Crescent terrane rocks with lower-velocity Pacific Rim terrane rocks is mapped between the Survey Mountain and Leech River faults (Figure 6b). The contact of Crescent terrane with Pacific Rim terrane is mapped as a north dipping velocity contrast F3 (Figures 7c and 7d).

6.3.3. Wrangellia

[32] Higher velocities mapped northeast of the Survey Mountain fault correlate with Wrangellia rocks (Figure 6b). Higher-velocity Wrangellia rocks (6.5–6.7 km/s) are mapped beneath Texada Island at a depth of about 4 km (Figure 7a). Velocities of Wrangellia rocks west of the Cowichan Fold and Thrust Belt (CFTB) are less than those observed to the east and possibly represent different lithologies (Figures 6e and 6f). Wrangellia rocks with a velocity close to 6.5 km/s form the basement of the Georgia basin in the Strait of Georgia (Figures 7a and 7b).

6.3.4. Wrangellia/Coast Plutonic Complex Suture

[33] The subsurface location of the contact between Wrangellia and the Coast Plutonic Complex probably lies beneath the Strait of Georgia [*Clowes et al.*, 1997; *Mulder*

and Rogers, 1998; *Spence and McLean*, 1998]. A SW dipping velocity contrast F4 is imaged northeast of the Strait of Georgia which may reflect this boundary (section P3, Figure 7c). This contact is inferred from relatively low velocities (<6.5 km/s) observed on the eastern margin of the Strait of Georgia compared to those on the western margin (>6.5 km/s) at the same depths. The SW dip of F4 suggests that Wrangellia terrane rocks were down-faulted against rocks of the Coast Plutonic Complex.

6.3.5. San Juan Islands

[34] Structures in the San Juan Islands result mainly from early Tertiary thrust faulting within sedimentary, volcanic, and metamorphic rocks [*Brandon et al.*, 1988]. North of Darrington-Devils Mountain fault, the San Juan Islands are underlain by a north oriented high-low-high structure in the 5.5 km/s isovelocity map (Figure 8a); these highs possibly represent upthrust blocks. The southern end of the Georgia basin is bounded by a velocity high beneath the San Juan Islands, south of the velocity contrast F2 (Figure 7b).

6.3.6. Possible Crustal Faults

[35] Several possible active crustal faults have been identified from subsurface velocity contrasts lying close to microseismicity clusters. Along the eastern margin of the Strait of Georgia, a velocity contrast across F1 (Figure 7a) coincides with a change of slope in the basin floor and with a cluster of microearthquake activity. The hypocenter of the M4.6 event of June 1997 [*Cassidy et al.*, 2000] also lies close to F1. Velocity contrasts across F5 and F6 east of the Leech River fault lie close to locations of microearthquake activity (Figure 7e). A velocity contrast across the Cowichan Fold and Thrust Belt places higher velocity rocks to the east of this belt than to the west (Figures 6e and 6f). This contrast may also reflect a lithological boundary within Wrangellia. In southern Vancouver Island, a velocity contrast between higher-velocity Wrangellia rocks to the northeast and lower-velocity Pacific Rim rocks to the southwest (Figure 6b) may represent a subsurface expression of the Survey Mountain fault.

6.3.7. Seismicity

[36] Four clusters of microseismicity (A–D in Figure 8b) are observed in the central and western Strait of Georgia. At cluster B, on the southern edge of the Nanaimo subbasin, seismicity peaks where the NW trend of the CFTB is intersected by the east trending high. A similar relation is observed at the east trending Devils Mountain fault (cluster A). In southwestern Georgia basin, micro-earthquake activity is limited to west of the Outer Island fault (cluster C). Microseismicity at the pronounced east trending structure in the Nanaimo subbasin (cluster D) appears to represent the northern limit of this major NW–SE microearthquake trend.

7. Summary

[37] A 3-D velocity model for southwestern British Columbia was constructed by tomographic inversion of first arrival travel times from the 1998 SHIPS experiment. The velocity model provides excellent constraints on the upper crustal velocity structure in SW British Columbia and adjacent Washington, and images four major basins. The WNW trending elongate Clallam basin, floored by Crescent Formation, is mapped in the Strait of Juan de Fuca with a maximum thickness of 5–6 km. The fault-bounded Sequim and Port Townsend basins are mapped in the eastern Strait of Juan de Fuca. In the southeastern end of the Georgia basin, the thickness of Cretaceous and younger sedimentary rocks is approximately 9 km, whereas in the northwestern end of the Georgia basin its maximum thickness is approximately 4 km. The locations and shapes of the basins spatially correlate with prominent gravity anomaly lows.

[38] The velocity model also defines the geometry of accreted terranes in the upper crust. A strong NW trending velocity discontinuity mapped along the western flank of the Strait of Georgia is possibly associated with the Cowichan Fold and Thrust Belt and Outer Islands fault. The volcanic Crescent terrane (Metchosin igneous complex) underlies extensive areas of southern Vancouver Island and the Strait of Juan de Fuca. Within the Crescent terrane basement, velocities >7.0 km/s likely delineate gabbro facies. In the Strait of Georgia, earthquake clusters define a NW trend, which corresponds approximately to lateral velocity contrasts in the subsurface. Microearthquakes are localized to the intersection of several east trending structural highs with this NW trend. This pattern suggests that structural styles observed in Puget Lowland extend northward to Vancouver.

[39] **Acknowledgments.** M. Fisher of the U.S. Geological Survey organized the SHIPS experiment that acquired the data used in this study. Anne Tréhu of the Oregon State University organized the northern Olympic peninsula stations for the SHIPS experiment. We thank Anne Tréhu, John Hole, and Robert Crosson for their helpful reviews of this paper. An earlier version of the manuscript was improved by reviews from Richard Blakely and Andy Calvert. This research was supported by a Natural Sciences and Engineering Research Council (NSERC) of Canada research grant. Geological Survey of Canada Contribution 2003120.

References

Brandon, M. T., D. S. Cowan, and J. A. Vance (1988), The Late Cretaceous San Juan Thrust system, San Juan Islands, Washington, *Spec. Pap. Geol. Soc. Am.*, *221*, 81 pp.

Brocher, T. M., and N. I. Christensen (2001), Density and velocity relationships for digital sonic and density logs from coastal Washington and laboratory measurements of Olympic peninsula mafic rocks and greywackes, *U.S. Geol. Surv. Open File Rep., 01–264*, 39 pp.

Brocher, T. M., and A. L. Ruebel (1998), Compilation of 29 sonic and density logs from 23 oil test wells in western Washington State, *U.S. Geol. Surv. Open File Rep., 98–249*, 41 pp.

Brocher, T. M., et al. (1999), Wide-angle seismic recordings from the 1998 Seismic Hazards Investigation of Puget Sound (SHIPS), western Washington and British Colombia, *U.S. Geol. Surv. Open File Rep., 99–314*, 110 pp.

Brocher, T. M., T. Parsons, R. A. Blakely, N. I. Christensen, M. A. Fisher, R. E. Wells, and the SHIPS Working Group (2001), Upper crustal structure in Puget Lowland, Washington: Results from 1998 Seismic Hazards Investigation in Puget Sound, *J. Geophys. Res.*, *106*, 13,541–13,564.

Cassidy, J. F., G. C. Rogers, and F. Waldhauser (2000), Characterization of active faulting beneath the Strait of Georgia, British Columbia, *Bull. Seismol. Soc. Am.*, *90*, 1188–1199.

Christensen, N. I., and W. D. Mooney (1995), Seismic velocity structure and composition of the continental crust: A global view, *J. Geophys. Res.*, *100*, 9761–9788.

Clowes, R. M., M. Brandon, A. G. Green, C. J. Yorath, A. Sutherland-Brown, E. R. Kanasewich, and C. S. Spencer (1987), LITHOPROBE southern Vancouver Island: Cenozoic subduction complex imaged by deep seismic reflections, *Can. J. Earth Sci.*, *24*, 31–51.

Clowes, R. M., D. J. Baird, and S. A. Dehler (1997), Crustal structure of the Cascadia subduction zone, southwestern British Columbia, from potential field and seismic studies, *Can. J. Earth Sci.*, *34*, 317–335.

Engebretson, D. C., A. Cox, and R. G. Gordon (1985), Relative motions between oceanic and continental plates in the Pacific Basin, *Spec. Pap. Geol. Soc. Am.*, *206*, 59 pp.

England, T. D. J., and R. M. Bustin (1998), Architecture of the Georgia Basin, southwestern British Columbia, *Bull. Can. Pet. Geol.*, *46*, 288–320.

England, T. D. J., and T. J. Calon (1991), The Cowichan fold and thrust system, Vancouver Island, southwestern British Columbia, *Geol. Soc. Am. Bull.*, *103*, 336–362.

Fisher, M. A., et al. (1999), Seismic survey probes urban earthquake hazards in Pacific Northwest, *Eos Trans. AGU*, *80*(2), 13, 16–17.

Hearn, T. M., and J. F. Ni (1994), *Pn* velocities beneath continental collision zones: The Turkish-Iranian Plateau, *Geophys. J. Int.*, *117*, 273–283.

Humphreys, E. D., and R. W. Clayton (1990), Tomographic image of the southern California mantle, *J. Geophys. Res.*, *95*, 19,725–19,746.

Hyndman, R. D. (1995), The Lithoprobe corridor across the Vancouver Island continental margin: The structural and tectonic consequences of subduction, *Can. J. Earth Sci.*, *32*, 1777–1802.

Hyndman, R. D., and K. Wang (1993), Thermal constraints on the zone of major thrust earthquake failure: The Cascadia subduction zone, *J. Geophys. Res.*, *98*, 2039–2060.

Johnson, S. Y., C. J. Potter, J. M. Armentrout, J. J. Miller, C. Finn, and C. S. Weaver (1996), The southern Whidbey Island fault: An active structure in the Puget Lowland, Washington, *Geol. Soc. Am. Bull.*, *108*, 334–354.

Khazaradze, G., A. Qamar, and H. Dragert (1999), Tectonic deformation in western Washington from continuous GPS measurements, *Geophys. Res. Lett.*, *26*, 3153–3156.

Massey, J. E. (1986), The Metchosin Igneous Complex, southern Vancouver Island: Ophiolite stratigraphy developed in an emergent setting, *Geology*, *14*, 602–605.

McMechan, G. A., and G. D. Spence (1983), *P*-wave velocity structure of the Earth's crust beneath Vancouver Island, *Can. J. Earth Sci.*, *20*, 742–752.

Monger, J. W. H. (1990), Georgia Basin—Regional setting and adjacent Coast Mountains geology, British Columbia, *Current Research, Part F, Paper 90-1F*, pp. 95–108, Geol. Surv. of Can., Ottawa, Ont.

Monger, J. W. H., R. A. Price, and D. J. Tempelman-Kluit (1982), Tectonic accretion and the origin of the two major metamorphic and plutonic welts in the Canadian Cordillera, *Geology*, *10*, 70–75.

Mosher, D. C., J. F. Cassidy, C. Lowe, Y. Mi, R. D. Hyndman, G. C. Rogers, and M. A. Fisher (2000), Neotectonics in the Strait of Georgia: Tentative correlation of seismicity with shallow geologic structure in southwestern British Columbia, *Current Research, 2000-A22*, pp. 1–9, Geol. Surv. of Can., Ottawa, Ont.

Mulder, T. L., and G. C. Rogers (1998), Poisson's ratio in southwestern British Columbia, program and abstracts, Abstract A131, Can. Geophys. Union, Quebec City, Canada.

Muller, J. E. (1977), Evolution of the Pacific Margin, Vancouver Island, and adjacent regions, *Can. J. Earth Sci.*, *14*, 2062–2085.

Muller, J. E. (1980), Chemistry and origin of Eocene Metchosin Volcanics, Vancouver Island, British Columbia, *Can. J. Earth Sci.*, *17*, 199–209.

Parsons, T. J., J. McCarthy, W. M. Kohler, C. J. Ammon, H. M. Benz, J. A. Hole, and E. E. Criley (1996), Crustal structure of the Colorado Plateau, Arizona: Application of new long-offset seismic data analysis techniques, *J. Geophys. Res.*, *101*, 11,173–11,194.

PASSCAL (1991), Users guide, A guide to planning experiments using PASSCAL Instruments, Inc. Res. Inst. for Seismol., Washington, D. C.

Ramachandran, K. (2001), Velocity structure of S.W. British Columbia and N.W. Washington from 3-D non-linear seismic tomography, Ph.D. thesis, Univ. of Victoria, Victoria, B. C., Canada.

Rogers, G. C., and H. S. Hasegawa (1978), A second look at the British Columbia earthquake of 23 June, 1946, *Bull. Seismol. Soc. Am.*, *68*, 653–676.

Spence, G. D., and N. A. McLean (1998), Crustal seismic velocity and density structure of the Intermontane and Coastal belts, southwestern Cordillera, *Can. J. Earth Sci.*, *35*, 1365–1379.

Spence, G. D., R. M. Clowes, and R. M. Ellis (1985), Seismic structure across the active subduction zone of western Canada, *J. Geophys. Res.*, *90*, 6754–6772.

Toomey, D. R., S. C. Solomon, and G. M. Purdy (1994), Tomographic imaging of the shallow crustal structure of the East Pacific Rise at 9°30′N, *J. Geophys. Res.*, *99*, 24,135–24,157.

Tréhu, A. M., T. M. Brocher, K. C. Creager, M. A. Fisher, L. Preston, and G. D. Spence (2002), Geometry of the subducting Juan de Fuca Plate: New constraints from SHIPS98, in *The Cascadia Subduction Zone and Related Subduction Systems—Seismic Structure, Intraslab Earthquakes and Processes, and Earthquake Hazards*, edited by S. Kirby, K. Wang, and S. Dunlop, *Open File 4350*, pp. 25–32, Geol. Surv. of Can., Ottawa, Ont.

Vidale, J. E. (1990), Finite-difference calculation of traveltimes in three dimensions, *Geophysics*, *55*, 521–526.

Van Wagoner, T. M., R. S. Crosson, K. C. Creager, G. Medema, L. Preston, N. P. Symons, and T. M. Brocher (2002), Crustal structure and relocated earthquakes in the Puget Lowland, Washington, from high-resolution seismic tomography, *J. Geophys. Res.*, *107*(B12), 2381, doi:10.1029/2001JB000710.

Wang, K., T. Mulder, G. C. Rogers, and R. D. Hyndman (1995), Case for low coupling stress on the Cascadia subduction fault, *J. Geophys. Res.*, *100*, 12,907–12,918.

Williams, R. A., W. J. Stephenson, J. K. Odum, and D. M. Worley (2001), Site response related shallow *P*- and *S*-wave velocity measurements in Seattle, and on the Crescent Formation near Olympia Washington, paper presented at Annual Meeting, Seismol. Soc. of Am., San Francisco, Calif.

Zelt, C. A., and P. J. Barton (1998), Three-dimensional seismic refraction tomography: A comparison of two methods applied to data from the Faeroe Basin, *J. Geophys. Res.*, *103*(B4), 7187–7210.

Zelt, B. C., R. M. Ellis, C. A. Zelt, R. D. Hyndman, C. Lowe, G. D. Spence, and M. A. Fisher (2001), Three dimensional crustal velocity structure beneath the Strait of Georgia, British Columbia, *Geophys. J. Int.*, *144*, 695–712.

T. M. Brocher, U.S. Geological Survey, MS 977, 345 Middlefield Road, Menlo Park, CA 94025, USA. (brocher@usgs.gov)

S. E. Dosso and G. D. Spence, School of Earth and Ocean Sciences, University of Victoria, Victoria, B.C., Canada V8W 3P6. (sdosso@uvic.ca; gspence@uvic.ca)

R. D. Hyndman and K. Ramachandran, Pacific Geoscience Centre, Geological Survey of Canada, 9860 W Saanich Road, Sidney, B.C., Canada V8L 4B2. (hyndman@pgc.nrcan.gc.ca; kramacha@nrcan.gc.ca)

C. A. Zelt, Rice University, Department of Earth Science, MS-126 P.O. Box 1892, Houston, TX 77251-1892, USA. (czelt@rice.edu)